JOURNAL OF AIRCRAFT
Vol. 41, No. 6, November–December 2004

Aeroelastic Modeling of Trailing-Edge-Flap Helicopter Rotors Including Actuator Dynamics

Jinwei Shen* and Inderjit Chopra†
University of Maryland, College Park, Maryland 20742

The effect of actuator dynamics on a helicopter rotor with trailing-edge flaps for vibration control is investigated. Trailing-edge flap, actuator, and elastic rotor blade equations of motion are formulated using Hamilton's variational principle. The coupled nonlinear, periodic equations are solved using finite elements in space and time. The baseline correlation study is based on wind-tunnel test data for a typical five-bladed bearingless rotor system. Good agreement is seen for the blade flap bending, chord bending, and torsion moments. It is shown that actuator dynamics cannot be neglected for a trailing-edge flap system with torsionally soft actuators. The parametric study performed using both coupled flap/actuator model and prescribed flap motion model indicated that the placement of trailing-edge flaps at 78% radius resulted in minimum flap input for this rotor. The vibration reduction level and trend are close between the predictions of both models at different forward speeds. Control inputs predicted by the coupled model show less sensitivity to the forward speed than that of prescribed model.

Nomenclature

a = lift curve slope
C_h = flap hinge moment coefficient
c = blade chord
c_a = actuator torsional damping
d = offset of flap hinge from blade elastic axis
e = flap leading-edge location aft of midchord, in semichords
F_x = N_b/rev longitudinal vibratory hub shear
F_y = N_b/rev lateral vibratory hub shear
F_z = N_b/rev vertical vibratory hub shear
H = flap hinge moment (positive flap down)
I_f = flap second mass moment of inertia about flap hinge, $\int\int y_f{}^2\,\mathrm{d}m$
J = scalar nondimensional vibration objective function
k_a = actuator torsional stiffness
l = offset of flap hinge from flap leading edge
l_f = flap length
M_x = N_b/rev roll vibratory hub moment
M_y = N_b/rev pitch vibratory hub moment
S_f = flap first mass moment of inertia about flap hinge, $\int\int y_f\,\mathrm{d}m$
T = kinetic energy
T_{1-29} = Theodorsen flap constants
U = strain energy
U_p = downwash velocity
U_t = air velocity tangential to blade chord
u = blade elastic axial displacements
v = blade elastic lag displacements
W = virtual work
w = blade elastic flap displacements
x = blade spanwise position
α = angle of attack
β_p = blade precone angle
γ = lock number
ΔL = flap incremental lift (positive up)
ΔM = flap incremental pitching moment (positive airfoil leading edge up)
δ = variation
δ_a = actuator input (positive flap down)
δ_f = flap deflection (positive flap down)
θ_0 = rigid pitch angle
ξ = blade modal response
$\hat{\phi}$ = blade elastic twist
ψ = azimuth angle

Subscripts

a = actuator
b = blade
D = deformed blade coordinate
F = trailing-edge flap coordinate
f = trailing-edge flap
H = trailing-edge flap hinge coordinate

Superscripts

$'$ = d/dx
$\star$ = $d/d\psi$
$\star\star$ = $d^2/d\psi^2$

Introduction

HELICOPTER rotors are susceptible to high vibrations, because flexible rotor blades operating in an unsteady aerodynamic environment result in complex aeroelastic couplings. Higher harmonic control (HHC) and individual blade control (IBC) have been shown to be effective in minimizing vibration but at a considerable weight penalty and system complexity.[1] In HHC and IBC systems, blades are feathered at higher harmonics of rotational speed, generating new unsteady airloads that if properly phased can cancel some of the original vibratory loads. Recently, with the emergence of smart material actuators, there have been growing activities to minimize vibration actively with trailing-edge flaps. Such a control system is expected to be a compact, lightweight, low-actuation-power, and high-bandwidth device that can be used for multifunctional roles such as vibration and noise suppression,[2] aeromechanical stability improvement,[3,4] rotor performance enhancement,[5,6] and swashplateless primary rotor control.[7] A variety of comprehensive rotorcraft analyses[8–10] have examined the performance of

Presented as Paper 2000-1622 at the AIAA/ASME/ASCE/AHS 41st Structures, Structural Dynamics, and Materials Conference, Anaheim, CA, 6 April 2000; received 26 July 2002; revision received 15 January 2004; accepted for publication 16 January 2004.

*Graduate Research Assistant, Alfred Gessow Rotorcraft Center, Department of Aerospace Engineering. Member AIAA.
†Alfred Gessow Professor and Director, Alfred Gessow Rotorcraft Center, Department of Aerospace Engineering. Fellow AIAA.

trailing-edge flaps for active vibration control in rotorcraft. However, most of these analyses incorporated prescribed flap motion and thereby neglected the dynamics of the actuators. This paper will address that issue.

Trailing-edge flaps have long been used as control devices in the fixed-wing community. Recently, trailing-edge flaps driven by smart material actuation have been an active research topic both experimentally and analytically. A large variety of Froude-scale and Mach-scale rotor models with various actuation schemes have been proposed and to a certain extent implemented. Vibration reduction has been demonstrated experimentally.[2] In analytical simulations, Millott and Friedmann[8] investigated servo flaps using a flexible blade model and modified Theodorsen aerodynamics. The servo-flap system was found to be just as effective as conventional multicyclic pitch control but with greatly reduced power requirements. The study included parametric studies of flap size, flap location, and blade torsional stiffness. The flap location was determined to be a significant design parameter. Milgram and Chopra[9,10] presented a comprehensive study based on the University of Maryland Advanced Rotorcraft Code (UMARC) using a compressible unsteady aerodynamic model[11] and the Bagai–Leishman free-wake model.[12] The analytical results were validated with wind-tunnel experimental data.[5] The Milgram and Chopra study indicates the feasibility of a 10% span, 20% chord trailing-edge flap, with ±5 deg flap travel, in reducing vibratory hub loads. The parametric design study examined the influence of flap system design parameters such as flap length and chord, spanwise location, and controller weighting parameters. The flap length and chord were found to be of less importance because the controller automatically adjusts for changes in flap authority by varying the input amplitudes. The flap spanwise location was found to be an important parameter. Myrtle and Friedmann[13] presented a rotor code for the active flap using an unsteady aerodynamic model for airfoil/flap based on a rational function approximation approach. Similar levels of vibration reduction are obtained when using quasi-steady Theodorsen aerodynamics and the new unsteady aerodynamic model. Unsteady aerodynamics, including free-wake modeling, was shown to be important for obtaining flap actuation power requirements. Straub and Hassan[14] and Straub and Charles[15] modified the comprehensive code CAMRAD/JA to account for the aerodynamics of blade sections with a trailing-edge flap and a simple model of actuator dynamics. The flap aerodynamics was modeled with an approximation of potential flow thin airfoil theory or with the use of a two-dimensional airfoil section table lookup. The CAMRAD II[16] code presented the ability to model the fully coupled blade/flap aerodynamics and dynamics. The steady flap aerodynamics is modeled using a two-dimensional airfoil table lookup. Incompressible unsteady loads are obtained using modified classical two-dimensional airfoil/flap theory.[17] Predicted results from CAMRAD/JA and CAMRAD II were compared for blades without flaps and for blades with prescribed flap motion.[15] The study showed that CAMRAD/JA captured the overall rotor response as well as trailing-edge flap loads with sufficient fidelity and that CAMRAD II predicated more accurate blade and flap loads.

For most of the previous trailing-edge flap analyses, the actuator dynamics was neglected. The principal objective of this paper is to present a comprehensive rotor aeroelastic analysis with trailing-edge flap including actuator dynamics.

Analytical Model

A comprehensive analysis for a rotor with active control flaps was formulated by Milgram et al.[9] and incorporated into UMARC. This analysis modeled the trailing-edge flap as a structural dynamic element with prescribed motion at the hinge located at the leading edge of the flap. It included flap inertia and aerodynamics but neglected the actuator dynamics. The present study extends that analysis by including actuator dynamics. The actuator and flap are modeled as two separate structural dynamic elements with the flap hinge located at an arbitrary chordwise portion of the flap.

The baseline rotor analysis is taken from UMARC.[18] The blade is assumed to be an elastic beam undergoing flap bending, lag bending, elastic twist, and axial deformation. The derivation of the coupled blade/actuator/trailing-edge flap equations of motion is based on Hamilton's variational principle generalized for a nonconservative system:

$$\delta\Pi = \int_{t_1}^{t_2} (\delta U - \delta T - \delta W)\,\mathrm{d}t = 0 \tag{1}$$

where δU is the variation of the elastic strain energy, δT is the variation of the kinetic energy, and δW is the work done by nonconservative forces. The blade, actuator, and trailing-edge flap contribute to the following energy expressions:

$$\delta U = \delta U_b + \delta U_f + \delta U_a \tag{2}$$

$$\delta T = \delta T_b + \delta T_f + \delta T_a \tag{3}$$

$$\delta W = \delta W_b + \delta W_f + \delta W_a \tag{4}$$

The trailing-edge flap coordinate system is shown in Fig. 1.

Structural Modeling

The actuator is modeled by a torsional spring and a torsional damper, which connect the flap with the baseline blade at a hinge located at an arbitrary chordwise portion of flap. The flap motion is indirectly controlled via base motion of the torsional spring (Fig. 2). The actuator mass is lumped into the baseline blade mass. The flap is assumed to be sectionally rigid and undergoes the same flap bending, lag bending, elastic twist, and axial deformation as the baseline blade but with an additional degree of freedom—flap torsional deflection. The blade sectional structural properties reflect the entire section, including actuator and trailing-edge flap. The variation of the strain energy of the baseline blade δU_b is not changed by the actuator and flap motion. The variation of the strain energy of actuator and flap are

$$\delta U_a = k_a \cdot (\delta_f - \delta_a) \cdot \delta(\delta_f) \tag{5}$$

$$\delta U_f = 0 \tag{6}$$

where δ_f is the angular deflection of the flap with respect to the blade and δ_a is the actuator angular deflection that is prescribed (Fig. 2).

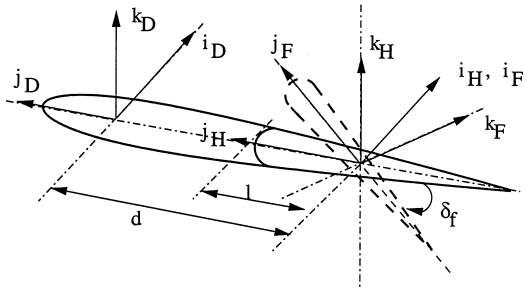

Fig. 1 Trailing-edge flap coordinate system.

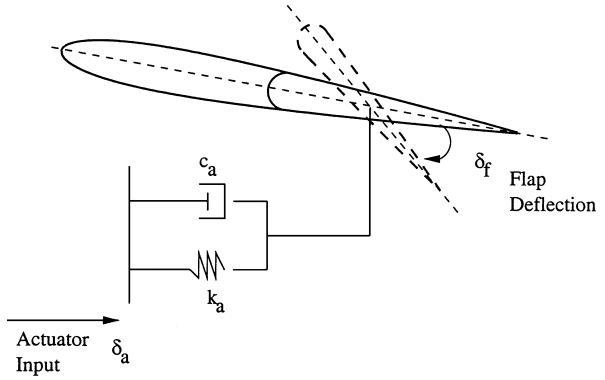

Fig. 2 Trailing-edge flap and actuator system.

The incremental variation of the kinetic energy of the baseline blade due to the flap motion is expressed as follows:

$$\delta(\Delta T_b) = \int_0^{l_f} (\Delta T_v \cdot \delta v + \Delta T_w \cdot \delta w + \Delta T_{\hat{\phi}} \cdot \delta\hat{\phi} + \Delta T_{v'} \cdot \delta v' + \Delta T_{w'} \cdot \delta w')\,\mathrm{d}x \tag{7}$$

where

$$\Delta T_v = -S_f \cdot \left(\delta_f \dot{\theta}_0^2 \sin\theta_0 - \hat{\phi}\cos\theta_0 \ddot{\delta}_f - \delta_f \cos\theta_0 \ddot{\delta}_f - \delta_f \cos\theta_0 \ddot{\theta}_0 - 2\dot{\theta}_0 \dot{\delta}_f \cos\theta_0 - \dot{\delta}_f^2 \cos\theta_0 + \delta_f \sin\theta_0 - \sin\theta_0 \ddot{\delta}_f\right) \tag{8}$$

$$\Delta T_w = -S_f \cdot \left(-\delta_f \dot{\theta}_0^2 \cos\theta_0 - \hat{\phi}\sin\theta_0 \ddot{\delta}_f - \delta_f \sin\theta_0 \ddot{\delta}_f - \delta_f \sin\theta_0 \ddot{\theta}_0 - 2\dot{\theta}_0 \dot{\delta}_f \sin\theta_0 - \dot{\delta}_f^2 \sin\theta_0 + \cos\theta_0 \ddot{\delta}_f\right) \tag{9}$$

$$\Delta T_{\hat{\phi}} = S_f \cdot \left(x\delta_f \sin\theta_0 \beta_p + 2d\delta_f \cos\theta_0^2 - d\delta_f + d\ddot{\delta}_f + \ddot{v}\delta_f \cos\theta_0 - \delta_f v\cos\theta_0 + \delta_f \sin\theta_0 \ddot{w}\right) - I_f \ddot{\delta}_f \tag{10}$$

$$\Delta T_{v'} = x S_f \delta_f \sin\theta_0 \tag{11}$$

$$\Delta T_{w'} = x S_f \delta_f \cos\theta_0 \tag{12}$$

where S_f is the flap first mass moment of inertia about the flap hinge ($S_f = \int\int y_f\,\mathrm{d}m$), I_f is the flap second mass moment of inertia about the flap hinge ($I_f = \int\int y_f{}^2\,\mathrm{d}m$) and l_f is the flap spanwise length.

The variation of the kinetic energy of the actuator and flap are

$$\delta T_a = 0 \tag{13}$$

$$\delta T_f = \int_0^{l_f} T_f \cdot \delta(\delta_f)\,\mathrm{d}x \tag{14}$$

where

$$T_f = F\left(S_f, I_f, x, v, \hat{\phi}, \dot{v}, \dot{w}, \ddot{v}, \ddot{w}, \dot{\hat{\phi}}, v', w', \dot{v}', \dot{w}', \ldots\right) \tag{15}$$

Aerodynamic Modeling

External aerodynamic forces on the blade contribute to the virtual work of the system. The incremental virtual work of the baseline blade due to the flap motion is expressed as follows. For simplicity of analysis, flap drag is currently neglected in the formulation:

$$\delta(\Delta W_b) = \int_0^{l_f} \left(\Delta L_w^A \cdot \delta w + \Delta M_{\hat{\phi}}^A \cdot \delta\hat{\phi}\right)\mathrm{d}x \tag{16}$$

$$\delta W_a = -c_a \cdot \left(\dot{\delta}_f - \dot{\delta}_a\right) \cdot \delta(\delta_f) \tag{17}$$

$$\delta W_f = \int_0^{l_f} H_\delta^A \cdot \delta(\delta_f)\,\mathrm{d}x \tag{18}$$

where c_a is actuator damping.

There are several available aerodynamic models for a flapped airfoil. The Hariharan–Leishman model[11] is incorporated into UMARC for trailing-edge flap studies.[9] This model is based on the indicial method and includes compressibility and unsteady effects. However, this model currently lacks the capability to model an aerodynamically balanced flap, which is often used to reduce the flap actuation force. Two trailing-edge-flap aerodynamic models are used in the present study. The first one is a quasi-steady model adapted from Theodorsen's theory,[17] which is capable of modeling the aerodynamical balance of flap, and the second one is a table lookup model based on test data. For the second model, the blade aerodynamic section coefficients (C_l, C_d, C_m) and flap aerodynamic coefficients (C_h) are looked up in the table for the current airfoil angle of attack, α, Mach number M, and trailing-edge flap deflection δ_f. For the airfoil without trailing-edge flap, a C81 format table lookup was used to define the blade aerodynamic coefficients. The Bagai–Leishman free-wake model[12] based on the pseudo-implicit predictor–corrector relaxation scheme was used to obtain induced in-flow distribution on the rotor disk.

For analytical flap aerodynamic models, the incremental lift ΔL, pitching moment ΔM, and trailing-edge-flap hinge moment H can be expressed in terms of blade and trailing-edge-flap deflections, velocities, and accelerations. These incremental forces and moments act in the blade deformed coordinate system and are subsequently transformed to the blade undeformed coordinate system respectively as ΔL_w^A, $\Delta M_{\hat{\phi}}^A$, and H_δ^A:

$$\Delta L = (\gamma/6a)\left[C_{l\delta_f} \cdot \delta_f \cdot U_t^2 + C_{l\dot{\delta}_f} \cdot \dot{\delta}_f \cdot U_t + C_{l\ddot{\delta}_f} \cdot \ddot{\delta}_f\right] \tag{19}$$

$$\Delta M = (\gamma/6a)\left[C_{m\delta_f} \cdot \delta_f \cdot U_t^2 + C_{m\dot{\delta}_f} \cdot \dot{\delta}_f \cdot U_t + C_{m\ddot{\delta}_f} \cdot \ddot{\delta}_f\right] \tag{20}$$

$$H = (\gamma/6a)\left[C_{h\delta_f} \cdot \delta_f \cdot U_t^2 + C_{h\dot{\delta}_f} \cdot \dot{\delta}_f \cdot U_t + C_{h\ddot{\delta}_f} \cdot \ddot{\delta}_f + C_{h\dot{h}} \cdot (-\dot{w}) \cdot U_t + C_{h\ddot{h}} \cdot (-\ddot{w}) + C_{h\alpha} \cdot (-U_t \cdot U_p) + C_{h\dot{\alpha}} \cdot \left(\dot{\theta}_0 + \dot{\hat{\phi}}\right) \cdot U_t + C_{h\ddot{\alpha}} \cdot \left(\ddot{\theta}_0 + \ddot{\hat{\phi}}\right)\right] \tag{21}$$

Using Theodorsen theory for aerodynamically balanced flaps, the coefficients are given by

$$C_{l\delta} = 2 \cdot (T_{10} - l \cdot T_{21}) \tag{22}$$

$$C_{l\dot{\delta}} = c \cdot l \cdot \left(-T_{10} - \sqrt{1 - e^2}\right) + \tfrac{1}{2}c \cdot (T_{11} - T_4) \tag{23}$$

$$C_{l\ddot{\delta}} = \tfrac{1}{4}c^2 \cdot (l \cdot T_4 - T_1) \tag{24}$$

$$C_{m\delta} = \left(-\tfrac{1}{2}\right)(l \cdot T_{22} + T_{15}) \tag{25}$$

$$C_{m\dot{\delta}} = \left(-\tfrac{1}{4}\right)c \cdot (l \cdot T_{23} + T_{16}) \tag{26}$$

$$C_{m\ddot{\delta}} = \left(-\tfrac{1}{8}\right)c^2 \cdot (l \cdot T_{24} + 2T_{13}) \tag{27}$$

$$C_{h\alpha} = l \cdot T_{20} - \tfrac{1}{2}T_{12} \tag{28}$$

$$C_{h\dot{\alpha}} = \tfrac{1}{4}c \cdot [l \cdot (2T_{20} - T_{25}) - T_{17} - T_{12}] \tag{29}$$

$$C_{h\ddot{\alpha}} = \tfrac{1}{8}c^2 \cdot (-l \cdot T_{24} - 2T_{13}) \tag{30}$$

$$C_{h\dot{h}} = l \cdot T_{20} - \tfrac{1}{2}T_{12} \tag{31}$$

$$C_{h\ddot{h}} = \tfrac{1}{4}c \cdot (T_1 - l \cdot T_4) \tag{32}$$

$$C_{h\delta} = -(1/\pi)l^2 \cdot \left(\tfrac{1}{2}T_{28} + T_{20}T_{21}\right) + (1/2\pi)l \cdot (T_{12}T_{21} - T_{26} + 2T_{20}T_{10}) - (1/2\pi) \cdot (T_{18} + T_{12}T_{10}) \tag{33}$$

$$C_{h\dot{\delta}} = (1/4\pi)c \cdot \left[l^2 \cdot (-2T_{20}T_{10} - T_{29}) + l \cdot (T_{12}T_{10} - T_{27} + T_{20}T_{11}) - T_{19} - \tfrac{1}{2}T_{12}T_{11}\right] \tag{34}$$

$$C_{h\ddot{\delta}} = (1/8\pi)c^2 \cdot \left(l^2 \cdot T_5 - l \cdot 2T_2 + T_3\right) \tag{35}$$

The air velocities are functions of blade motions; therefore, many of the aerodynamic terms in the virtual work are blade and flap motion dependent and contribute to the element matrices:

$$U_t = F(u, v, w, \hat{\phi}, \dot{v}, \dot{w}, \ddot{v}, \ddot{w}, v', w', \ldots) \tag{36}$$

$$U_p = F(v, w, \hat{\phi}, \dot{v}, \dot{w}, \dot{\hat{\phi}}, v', w', \ldots) \tag{37}$$

Coupled Blade/Actuator/Flap Equations

The blade is discretized into a number of beam elements. Each element consists of 15 degrees of freedom. These degrees of freedom are distributed over five element nodes (two boundary nodes and three interior nodes). There are six degrees of freedom at each element boundary node. These six degrees of freedom correspond to u, v, v', w, w', and $\hat{\phi}$. There are two internal nodes for elastic axial deflection u and one internal node for elastic twist $\hat{\phi}$. Between elements, there is continuity of displacement and slope for flap and lag bending deflections and continuity of displacement for elastic twist and axial deflections. This element ensures physically consistent linear variations of bending moments and torsional moments and quadratic variation of axial force within each element. Blade, actuator, and trailing-edge flap equations of motion are expressed into the modal space as follows:

$$\begin{bmatrix} \boldsymbol{M}_{bb} & \boldsymbol{M}_{bf} \\ \boldsymbol{M}_{fb} & \boldsymbol{M}_{ff} \end{bmatrix} \begin{Bmatrix} \ddot{\boldsymbol{\xi}} \\ \ddot{\delta}_f \end{Bmatrix} + \begin{bmatrix} \boldsymbol{C}_{bb} & \boldsymbol{C}_{bf} \\ \boldsymbol{C}_{fb} & \boldsymbol{C}_{ff} \end{bmatrix} \begin{Bmatrix} \dot{\boldsymbol{\xi}} \\ \dot{\delta}_f \end{Bmatrix} + \begin{bmatrix} \boldsymbol{K}_{bb} & \boldsymbol{K}_{bf} \\ \boldsymbol{K}_{fb} & \boldsymbol{K}_{ff} \end{bmatrix} \begin{Bmatrix} \boldsymbol{\xi} \\ \delta_f \end{Bmatrix} = \begin{Bmatrix} \boldsymbol{F}_{bb} \\ \boldsymbol{F}_{ff} \end{Bmatrix} \tag{38}$$

The coupled blade/actuator/trailing-edge flap equations that are solved using finite elements in space and time are nonlinear and periodic. Because the actuation force driving the flap is assumed to be periodic, the trailing-edge-flap response will also be periodic. Therefore, periodic boundary conditions are applied to the temporal elements.

Multicyclic Controller

A multicyclic controller[19] is used to determine the flap control inputs. This algorithm is based on minimization of an objective function,

$$J \equiv {z_n}^T W_z z_n + {\theta_n}^T W_\theta \theta_n + \Delta{\theta_n}^T W_{\Delta\theta} \Delta\theta_n \tag{39}$$

where z_n is a hub loads vector containing the cosine and sine coefficients of the N_b/rev fixed-system hub loads F_x, F_y, F_z, M_x, and M_y at time step n; θ_n and $\Delta\theta_n$ represent the harmonics of the control inputs and control rates, respectively. The diagonal matrices W contain weights for different harmonics of the vibration, W_z, the control inputs W_θ, and the control rates $W_{\Delta\theta}$.

The weighting matrices used in the present study are

$$\boldsymbol{W}_z = \begin{pmatrix} 0.040 & & & & & \\ & 0.023 & & & & \\ & & 1.0 & & & \\ & & & 0.440 & & \\ & & & & 0.136 & \end{pmatrix} \tag{40}$$

$$\boldsymbol{W}_\theta = 0 \tag{41}$$

$$\boldsymbol{\Delta W}_\theta = 0 \tag{42}$$

The weighting matrix W_z is selected to give a compromised consideration on the vibration level at the pilot seat, copilot seat, center of gravity, and Notar fan of the MD-900 Explorer based on a NASTRAN simulation. For the five-bladed rotor, the trailing-edge-flap inputs used in the present study are 4/rev, 5/rev, and 6/rev.

Results and Discussion

Before results of actuator dynamics modeling are presented, the predictive capability of UMARC for a baseline bearingless rotor without trailing-edge flaps is evaluated by correlating with wind-tunnel experimental data. Trailing-edge-flap airfoil aerodynamics coefficient predictions are then compared with wind-tunnel test data. With the fairly good correlation of UMARC baseline rotor modeling and the trailing-edge-flap aerodynamic model, the UMARC predictions including actuator dynamics are included in two parts: 1) investigation of coupling effect among blade, actuator, and trailing-edge flap; and 2) parametric study on flap spanwise location that includes actuator dynamics.

Table 1 MDART rotor properties

Property	Value
Rotor type	Bearingless
Number of blades	5
Rotor diameter	34 ft
Rotor speed	392 rpm
Chord	0.0492 R
Twist angle	−10 deg (nominal)
Solidity	0.078

Table 2 MDART blade natural frequencies

Parameter	UMARC, /rev	CAMRAD II (Ref. 15), /rev
Flap	1.04	1.05
	2.68	2.78
	4.62	4.57
Lag	0.68	0.61
	4.33	4.43
Torsion	6.18	5.95

Baseline Rotor (Without Trailing-Edge Flaps)

The predictive capabilities of UMARC for a bearingless rotor without trailing-edge flaps were evaluated by comparing calculated results with wind-tunnel test data for the McDonnell Douglas Advanced Rotor Technology (MDART).[20] The MDART rotor is a preproduction version of the MD-900 Explorer, a five-bladed bearingless rotor. Its design parameters are given in Table 1. Table 2 compares calculated rotating natural frequencies of the MDART rotor between the present analysis and CAMRAD II. Overall, good agreement is seen. The small discrepancy may be a result of different structural properties used in the analyses. For example, the present analysis assumes a snubber stiffness consistent with Ref. 21, whereas CAMRAD II results in Table 2 are based on a lower value.

The modeling of the baseline MD-900 rotor was correlated by comparing the flap, chord, and torsion structural moment distributions. The comparisons were performed for a simulated descent flight condition at an advance ratio of 0.2 with a 3.5-deg aft tip path plane angle and a thrust coefficient C_T/σ of 0.0774. The analysis utilized the wind-tunnel trim procedure: trimming to the prescribed thrust level with zero first harmonic blade flapping. Figure 3 shows that UMARC results for the baseline rotor are in good agreement with test data.

Validation of Aerodynamics Model of Trailing-Edge Flap Airfoil

This section presents the validation study of a trailing-edge-flap airfoil aerodynamics model by comparing the predictions with wind-tunnel test data. The test data are from a two-dimensional wind-tunnel test conducted in the NASA Langley 0.3-m Transonic Cryogenic Tunnel.[22] The goal was to identify a suitable trailing-edge-flap geometry for helicopter rotor aerodynamic/dynamic applications. Two pressure-instrumented models of the HH-06 (9.5% thick) and HH-10 (12% thick) airfoils having 35% chord integral plain trailing-edge flaps and different overhang lengths were tested.

The aerodynamic coefficient predictions using Theodorsen's model[17] are compared with wind-tunnel test data for the HH-06 airfoil in Fig. 4. The two-dimensional airfoil aerodynamic coefficients of lift, pitching moment, and hinge moment are compared with three trailing-edge flap deflections, namely neutral and 4 deg upward and downward, at different angles of attack. Good agreement is seen for the lift coefficient and fair agreement for pitching moment coefficient. Hinge moment coefficient predictions only qualitatively agree with the test data. Most of the difference between predictions and test data are a result of viscous effects at the hinge gap and flow separation effects.

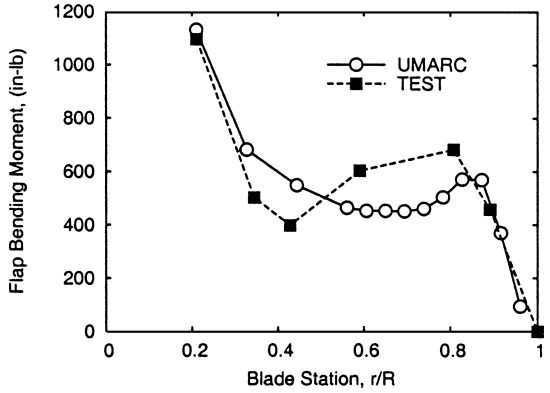

a) Flapwise bending moment

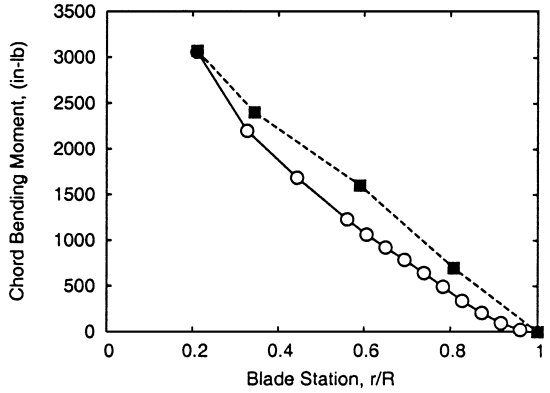

b) Chordwise bending moment

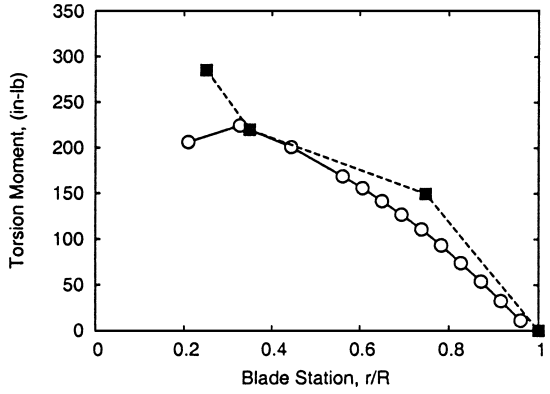

c) Torsional moment

Fig. 3 Measured and predicted structural moment distribution (half-peak-to-peak), advance ratio of 0.2, $C_T/\sigma = 0.0774$.

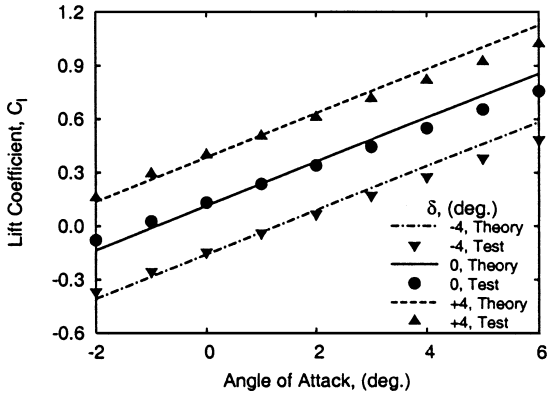

a) Lift coefficient

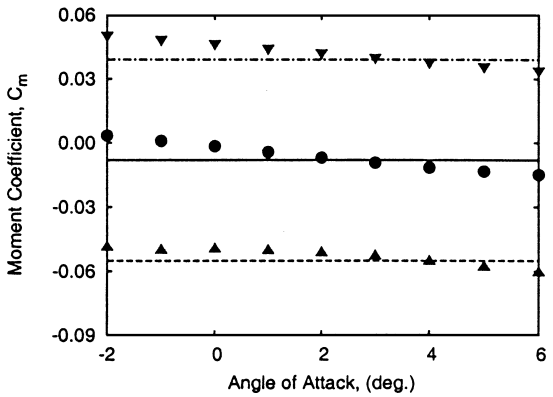

b) Moment coefficient

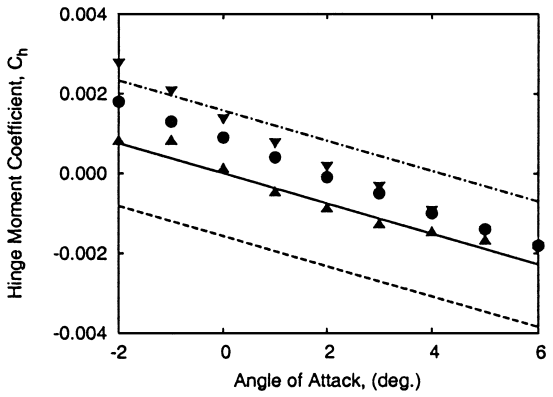

c) Hinge moment coefficient

Fig. 4 Measured and predicted aerodynamic coefficients of two-dimensional HH-06 airfoil with 0.35 plain trailing-edge flap (10% c overhang, $M = 0.20$).

Flap Analysis Including Actuator Dynamics

The following sections discuss calculated results from the UMARC analysis using analytical expressions for aerodynamic coefficients and with the inclusion of actuator dynamics using the fully coupled blade/actuator/flap analysis.

Figure 5 illustrates the coupling effect of actuator on resultant flap angle variation for one complete revolution for two different values of actuator stiffness. Three actuator stiffnesses were considered: 1) soft actuator (10% of the baseline actuator stiffness), 2) baseline actuator, and 3) rigid actuator (10 times that of the baseline actuator stiffness). Actuator input is $\delta_a = (2)$ deg $\cos(4\psi - 240$ deg). In the presence of actuator dynamics, flap deflection differs considerably from the actuator input for the trailing-edge flap system with the softer actuator. The flap deflection of the flap system with the rigid actuator is almost the same with the actuator input.

Parametric Study

Parametric studies have been conducted to investigate the impact of flap and actuator design on control authority and power

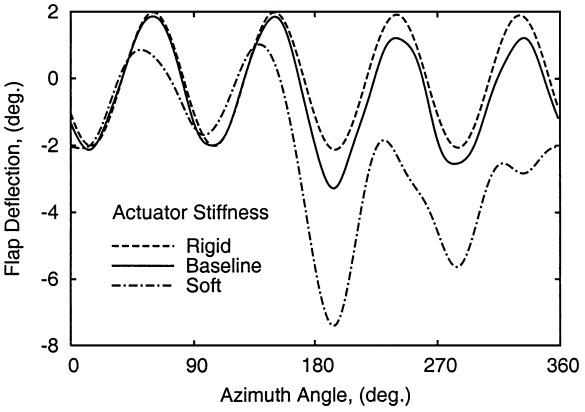

Fig. 5 Flap deflections with different actuator stiffness, advance ratio of 0.2, with actuator input $\delta_a = 2\cos(4\psi - 240$ deg).

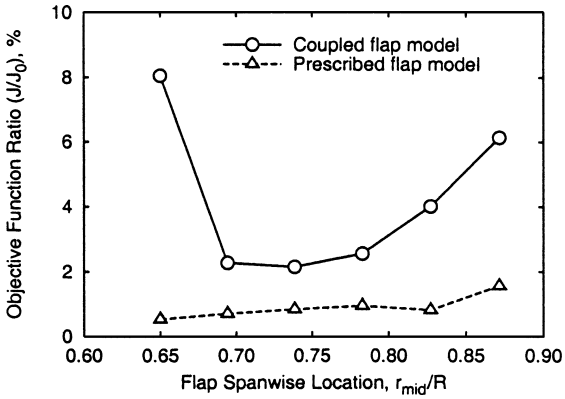

a) Objective function

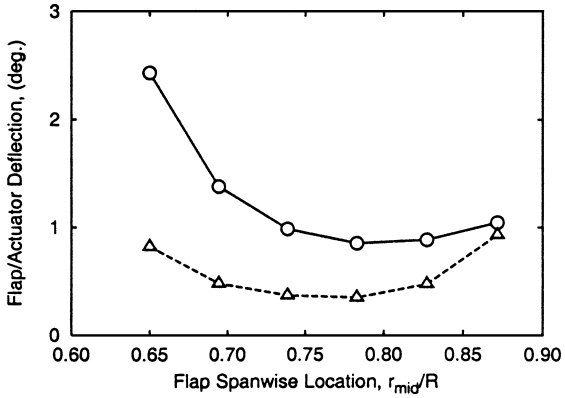

b) Flap/actuator deflection, half-peak-to-peak

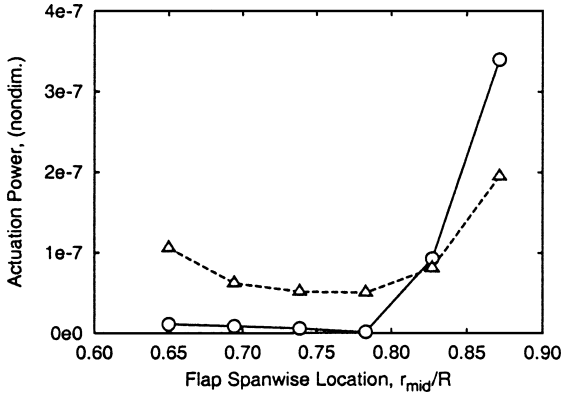

c) Actuation power

Fig. 6 Comparison of trailing-edge flap models (with and without actuator dynamics) for different flap locations, advance ratio of 0.3, $C_T/\sigma = 0.075$.

consumption. Key flap design parameters, such as flap spanwise length and chord and spanwise location, have been examined.[8,10] The goal of the present study is to investigate the coupling effect of actuator and flap dynamics on the selection of flap design parameters. The predictions of the present UMARC model, incorporating actuator dynamics, are compared with those of UMARC using prescribed flap motion. The multicyclic controller described earlier is used to provide the optimum flap control schedule. For the prescribed flap, the controller output is the flap deflection. In contrast, for the coupled blade/actuator/flap model, the controller output is the actuator input. The actual flap deflection is calculated by solving the coupled blade/flap/actuator equations.

The spanwise location of the trailing-edge flap is believed to be an important factor for the active control system.[8,10] To obtain an optimum flap spanwise location, the simulations are performed with different flap locations. The following results are calculated at an advance ratio 0.30 (123 kn) and for a selected C_T/σ of 0.075. They respectively represent the cruise speed and the nominal weight of MD-900.

The objective function reduction ratio is shown in Fig. 6a. The objective function predicted by using the coupled model achieved less vibration reduction overall than that of the prescribed model. Figure 6b illustrates the half-peak-to-peak values of control inputs for both models. The control inputs are the actuator motion for the coupled model and trailing-edge-flap motion for the prescribed model. The coupled model requires larger half-peak-to-peak control input than that of the prescribed model. The actuation power required is presented in Fig. 6c. Actuation power predicted with the coupled model shows a larger increase with the flap moving outboard than in the prescribed model. The optimum location of trailing-edge flaps (midspan) predicted for this rotor by both models is at 78% blade radius, where minimum actuation requirements are needed and sufficient vibration reduction is achieved.

The current MD-900 flap design parameters are shown in Table 3. With this flap system, simulations are performed using both the coupled flap/actuator model and the prescribed flap motion model

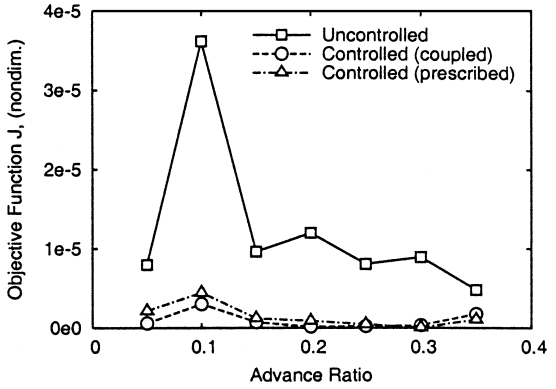

a) Objective function

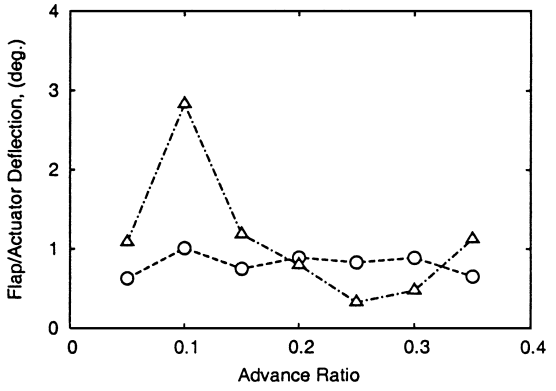

b) Flap/actuator deflection, half-peak-to-peak

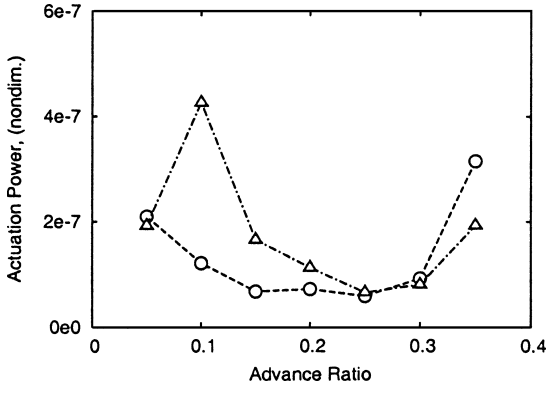

c) Actuation power

Fig. 7 Comparison of trailing-edge flap models at different forward speeds, advance ratio of 0.3, $C_T/\sigma = 0.075$, flap midspan location at 83% R.

at several advance ratios. The thrust level and shaft tilt angle are prescribed to simulate steady level flight conditions (Table 4). The uncontrolled and controlled objective functions predicted by both models are shown in Fig. 7a. Both models show that the controlled objective function reduces below 40% of the uncontrolled values for advance ratios from 0.05 to 0.35. The vibration reduction level and trend are close between the predictions of both models. Figure 7b shows the effect of actuation dynamics on the half-peak-to-peak

Table 3 MD-900 active trailing-edge flap properties

Property	Value
Flap type	Plain flap
Spanwise length	36 in. (0.18 R)
Chordwise size	35% (blade chord)
Flap midspan location	0.83 R
Flap hinge overhang	10% (airfoil chord)
Actuator stiffness	81.52 (ft-lb/rad)
Actuator damping	0.005 (ft-lb $\cdot$ rad^{-1} $\cdot$ s^{-1})

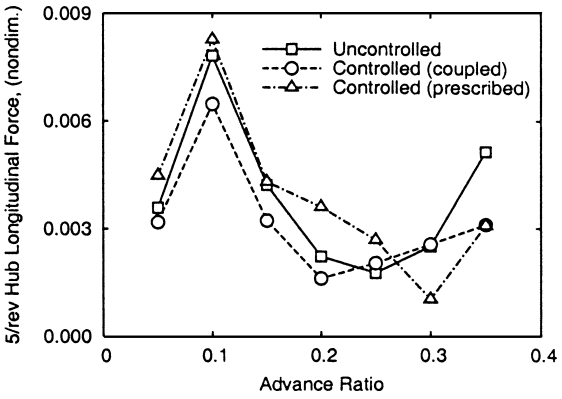

a) Longitudinal force

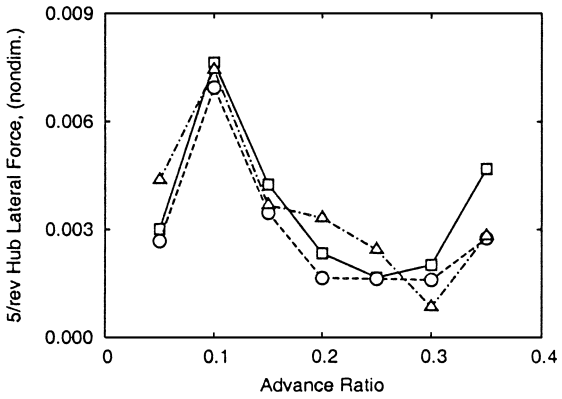

b) Lateral force

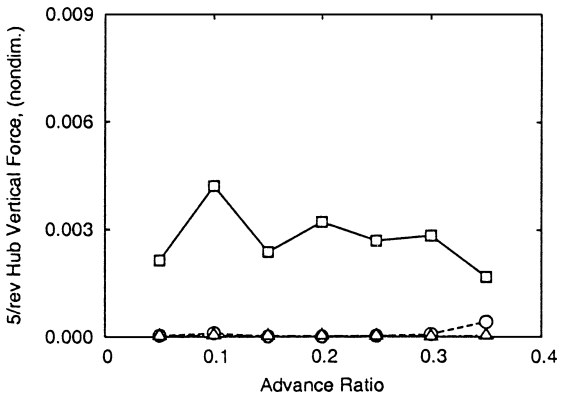

c) Vertical force

Fig. 8 5/rev hub forces.

Table 4 Prescribed shaft angles in different forward speeds positive is shaft tilt forward, $C_T/\sigma = 0.075$)

Advance ratio μ	Airspeed, kts	Shaft angle α_s, deg
0.05	21	0.5
0.10	41	1.1
0.15	62	2.6
0.20	82	4.9
0.25	103	6.9
0.30	123	8.8
0.35	144	10.9

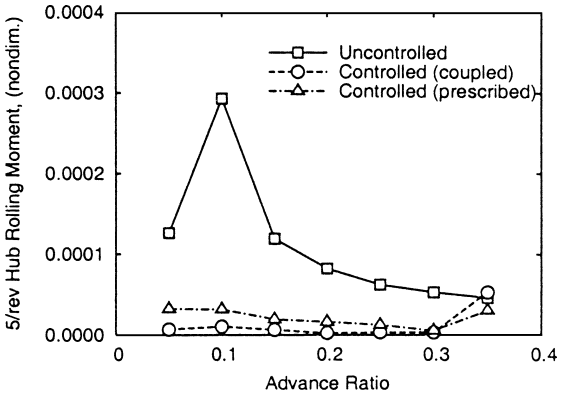

a) Rolling moment

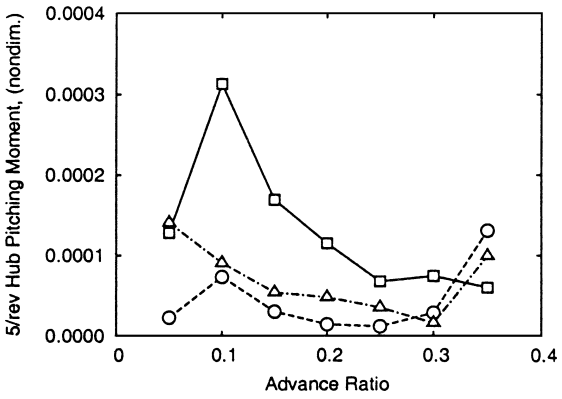

b) Pitching moment

Fig. 9 5/rev hub moments.

control input at different forward speeds. Control inputs predicted by the coupled model show less sensitivity to the forward speed than that of the prescribed model. Figure 7c presents the effect of actuation dynamics on the actuation power required. At low advance ratios, the prescribed model predicts a higher actuation power than that of the coupled model. However, at a high advance ratio of 0.35, the predictions of actuation power are higher using the coupled flap model than when using the prescribed model. The predicted 5/rev vibratory hub loads with both models are shown in Figs. 8 and 9. The 5/rev vibratory longitudinal force (Fig. 8a) and lateral force (Fig. 8b) with active control were either not reduced or were reduced slightly because of their small weighting in the objective function. The 5/rev vibratory vertical force (Fig. 8c) is almost reduced to zero because of its significant weighting in the objective functions. Figure 9a shows that hub rolling moments with active flap control predicted by both models are significantly reduced at advance ratios below 0.35. The predictions by coupled models show slightly higher reduction than that of the prescribed model except at an advance ratio of 0.35. Figure 9b shows that hub pitching moments with active flap control are also reduced at advance ratios below 0.35, but less vibration reduction is achieved compared to hub rolling moments. The predictions made by using coupled models show slightly higher reduction than those of the prescribed model at advance ratios below 0.30.

Summary

The system equations of the fully coupled blade/flap/actuator system were formulated using Hamilton's variational principle. The actuator and flap were modeled as two separate structural dynamic elements with the flap hinge located at an arbitrary chordwise portion of the flap. The blade/actuator/flap aerodynamic and inertial coupling effects were explicitly derived. The coupled equations were solved using finite elements in space and time. The impact of actuator dynamics on the control authorities and actuation requirements of a trailing-edge-flap system for helicopter vibration control was investigated.

A correlation study for the baseline bearingless rotor was performed using MDART wind-tunnel experimental data. Good agreement is seen for the blade flap bending, chord bending, and torsion moments. Aerodynamic coefficient predictions using Theodorsen's model were compared with wind-tunnel test data. Good agreement is seen for the lift coefficient and fair agreement for pitching moment coefficient. Hinge moment coefficient predictions only qualitatively agreed with the test data.

A large coupling effect resulting from actuator dynamics is seen with a soft actuator, resulting in flap deflections that differ considerably from the actuator input.

The parametric study conducted to examine flap location using both coupled and prescribed flap motion models showed that the trailing-edge flap was very effective in reducing 5/rev vibratory hub loads. Spanwise placement of the flap has a significant impact on actuation power requirement. Both coupled and prescribed flap models indicate that the placement of the flap midspan at 78% radius resulted in minimum flap input for this rotor. Numerical simulations were performed using both the coupled flap/actuator model and the prescribed flap motion model at several advance ratios. Both models showed that the objective function can be reduced to less than 40% of the uncontrolled objective function for advance ratios ranging from 0.05 to 0.35. The vibration reduction level and trend are close between the predictions of both models. Control inputs predicted by the coupled model show less sensitivity to the forward speed than those of prescribed model. Both models predicted maximum reductions in the 5/rev hub vertical force because of its significant weighting in the objective functions.

Acknowledgments

This work was supported by Boeing-Mesa under a (Defense Advanced Research Projects Agency) contract. The authors gratefully acknowledge Friedrich Straub (Boeing-Mesa) for making the design data and experimental results available as well as for providing valuable advice and assistance.

References

[1]Ham, N. D., "Helicopter Individual-Blade-Control and Its Applications," *Proceedings of the 39th Annual Forum of the American Helicopter Society*, American Helicopter Society, Alexandria, VA, 1983, pp. 613–623.

[2]Chopra, I., "Status of Application of Smart Structures Technology to Rotorcraft Systems," *Journal of the American Helicopter Society*, Vol. 45, No. 4, 2000, pp. 228–252.

[3]Celi, R., "Stabilization of Helicopter Blades with Severed Pitch Links Using Trailing-Edge Flaps," *Journal of Guidance, Control, and Dynamics*, Vol. 26, No. 4, 2003, pp. 585–592.

[4]Shen, J., and Chopra, I., "Aeroelastic Stability of Trailing-Edge Flap Helicopter Rotors," *Journal of the American Helicopter Society*, Vol. 48, No. 4, 2003, pp. 236–243.

[5]Straub, F. K., "Active Flap Control for Vibration Reduction and Performance Improvement," *Proceedings of the 51st Annual Forum of the American Helicopter Society*, American Helicopter Society, Alexandria, VA, 1995, pp. 381–392.

[6]Shen, J., Chopra, I., and Johnson, W., "Performance of Swashplateless Ultralight Helicopter Rotor with Trailing-Edge Flaps for Primary Flight Control," *Proceedings of the 59th Annual Forum of the American Helicopter Society*, American Helicopter Society, Alexandria, VA, 2003, p. 11.

[7]Shen, J., and Chopra, I., "A Parametric Design Study for a Swashplateless Helicopter Rotor with Trailing-Edge Flaps," *Journal of the American Helicopter Society*, Vol. 49, No. 1, 2004, pp. 43–53.

[8]Millott, T., and Friedmann, P., "Vibration Reduction in Helicopter Rotors Using an Actively Controlled Partial Span Trailing Edge Flap Located on the Blades," NASA TR CR 4611, June 1994.

[9]Milgram, J., Chopra, I., and Straub, F., "Rotors with Trailing Edge Flaps: Analysis and Comparison with Experimental Data," *Journal of the American Helicopter Society*, Vol. 43, No. 4, 1998, pp. 319–332.

[10]Milgram, J., and Chopra, I., "A Parametric Design Study for Actively Controlled Trailing Edge Flaps," *Journal of the American Helicopter Society*, Vol. 43, No. 2, 1998, pp. 110–119.

[11]Hariharan, N., and Leishman, J. G., "Unsteady Aerodynamics of a Flapped Airfoil in Subsonic Flow by Indicial Concepts," *Journal of Aircraft*, Vol. 33, No. 5, 1996, pp. 855–868.

[12]Bagai, A., and Leishman, J. G., "Rotor Free-Wake Modeling Using a Pseudo-Implicit Technique—Including Comparisons with Experimental Data," *Journal of the American Helicopter Society*, Vol. 40, No. 3, 1995, pp. 29–41.

[13]Myrtle, T. F., and Friedmann, P. P., "Vibration Reduction in Rotorcraft Using Actively Controlled Trailing Edge and Issue Related to Practical Implementation," *Proceedings of the 54th Annual Forum of the American Helicopter Society International*, American Helicopter Society, Alexandria, VA, 20–22 May 1998, pp. 602–619.

[14]Straub, F. K., and Hassan, A. A., "Aeromechanic Considerations in the Design of a Rotor with Smart Material Actuated Trailing Edge Flaps," *Proceedings of the 52nd Annual Forum of the American Helicopter Society*, American Helicopter Society, Alexandria, VA, 4–6 June 1996, pp. 704–714.

[15]Straub, F. K., and Charles, B. D., "Aeroelastic Analysis of Rotors with Trailing Edge Flaps Using Comprehensive Codes," *Journal of the American Helicopter Society*, Vol. 46, No. 3, 2001, pp. 192–199.

[16]Johnson, W., "Rotorcraft Dynamics Models for a Comprehensive Analysis," *Proceedings of the 54th Annual Forum of the American Helicopter Society International*, American Helicopter Society, Alexandria, VA, 20–22 May 1998, pp. 452–471.

[17]Theodorsen, T., and Garrick, I. E., "Nonstationary Flow About a Wing-Aileron-Tab Combination Including Aerodynamic Balance," NACA TR 736, 1942.

[18]Bir, G., and Chopra, I., "University of Maryland Advanced Rotor Code (UMARC) Theory Manual," Center for Rotorcraft Education and Research, Univ. of Maryland, College Park, MD, TR UM-AERO 94-18, July 1994.

[19]Johnson, W., "Self-Tuning Regulators for Multicyclic Control of Helicopter Vibration," NASA TR TP 1996, March 1982.

[20]McNulty, M., Jacklin, S., and Lau, B., "A Full-Scale Test of the McDonnell Douglas Advanced Bearingless Rotor in the NASA Ames 40- by 80-Ft Wind Tunnel," *Proceedings of the 49th Annual Forum of the American Helicopter Society*, American Helicopter Society, Alexandria, VA, 19–21 May 1993, pp. 1535–1544.

[21]Nguyen, K., Lauzon, D., and Anand, V., "Computation of Loads on the McDonnell Douglas Advanced Bearingless Rotor," *Proceedings of the 50th Annual Forum of the American Helicopter Society*, American Helicopter Society, Alexandria, VA, 11–13 May 1994, pp. 337–346.

[22]Hassan, A. A., Straub, F. K., and Noonan, K. W., "Experimental/Numerical Evaluation of Integral Trailing Edge Flaps for Helicopter Rotor Applications," *Proceedings of the 56th Annual Forum of the American Helicopter Society*, American Helicopter Society, Alexandria, VA, 2–4 May 2000, pp. 84–102.